DOI: 10.1002/cnma.201600300

Micromotors

Dynamics of Novel Photoactive AgCl Microstars and Their Environmental Applications

Juliane Simmchen,*[a, b] Alejandro Baeza,[c, d] Albert Miguel-Lopez,[a, f] Morgan M. Stanton,[a] Maria Vallet-Regi,[c, d] Daniel Ruiz-Molina,[b] and Samuel Sánchez[a, e, f]

Abstract: In the field of micromotors many efforts have been taken to find a substitute for peroxide as fuel. While most approaches turn towards other toxic high energy chemicals such as hydrazine, we introduce here an energy source that is widely used in nature: light. Light is an ideal source of energy and some materials, such as AgCl, have the inherent property to transform light energy for chemical processes, which can be used to achieve propulsion. In the case of silver chloride, one process observed after light exposure is surface modification, which leads to the release of ions, generating chemo-osmotic gradients. Here we present endeavors to use those processes to propel uniquely shaped micro-objects of microstar morphology with a high surface-to-volume ratio, study their dynamics and present approaches to go towards real environmental applications.

Introduction

Continuous energy conversion is required to propel micromotors. The most commonly employed method used with this aim is the conversion of chemical energy from the degradation of high energy chemicals such as peroxide[1] or hydrazine.[2] However, many efforts are taken to find alternatives to these toxic components whenever applications such as biomedical or environmental remediation applications are envisaged.[3] Among them, enzymes open possibilities for more biocompatible fuels,[4] and alternatives routes such as surface-tension-driven propulsion due to the release of solvent have been investigated.[5] Light is an ideal source of energy and some materials are able to transform this energy directly by undergoing chemical changes so that no toxic chemicals are required.[6] For instance, Palacci et al. achieved peroxide degradation by hematite under light irradiation,[7] and peroxide-free approaches have been presented, for example, on TiO_2 structures[8] but the motion mechanism is not yet completely understood. The collective motion of the AgCl particles by UV light has also been studied.[9] Light exposure induces a surface modification of the particles due to a state change from ionized to metallic silver that creates a localized electrolyte gradient around the particle that results in self-diffusiophoresis.[10] The hypothesized degradation of AgCl is shown in Equation (1).

$$4\,AgCl + 2\,H_2O \xrightarrow{UV-\ light} 4\,Ag + 4\,H^+ + 4\,Cl^- + O_2 \qquad (1)$$

Ibele et al. found that AgCl particles with asymmetric shape move autonomously in deionized (DI) water when exposed to UV light.[9c] A more recent work analyses the motion patterns of silver chloride particles under UV light classifying them according to the interaction between neighboring particles as isolated, coupled or schooled particles.[9a]

Herein we describe the synthesis and study of new AgCl micromotors with novel microstar-shaped morphologies. Branched microstructures were obtained with a high surface-to-volume ratio, which is expected to facilitate the motion of the resulting structures due to the higher number of active sites. We show how these motors exhibit three different motion modes in the presence of UV, including translational, rocking, and rotational motion, which were quantified. We also

[a] Dr. J. Simmchen, A. Miguel-Lopez, Dr. M. M. Stanton, Dr. S. Sánchez
Smart NanoBioSystems
Max-Planck-Institut für Intelligente Systeme
Heisenbergstr. 3, 70569 Stuttgart (Germany)
E-mail: juliane.simmchen@tu-dresden.de
[b] Dr. J. Simmchen, Dr. D. Ruiz-Molina
Catalan Institute of Nanoscience and Nanotechnology (ICN2)
CSIC
and The Barcelona Institute of Science and Technology
Campus UAB, Bellaterra, 08193 Barcelona (Spain)
[c] Dr. A. Baeza, Prof. Dr. M. Vallet-Regi
Dep. de Química InorgánicayBioinorgánica
UCM
Plaza Ramón y Cajal s/n, Madrid (Spain)
[d] Dr. A. Baeza, Prof. Dr. M. Vallet-Regi
Centro de Investigación Biomédica en Red de Bioingeniería, Biomaterialesy-Nanomedicina (CIBER-BBN)
(Spain)
[e] Dr. S. Sánchez
Institució Catalana de Recerca i Estudis Avancats (ICREA), Pg.
Lluís Companys 23, 08010, Barcelona (Spain)
[f] A. Miguel-Lopez, Dr. S. Sánchez
Institut de Bioenginyeria de Catalunya (IBEC)
Baldiri I Reixac 10–12, 08028 Barcelona (Spain)■■Please check addresses match authors, particularly [f]■■

Supporting information for this article can be found under: http://dx.doi.org/10.1002/cnma.201600300.

demonstrate applications based on the intrinsic properties of AgCl, such as catalytic degradation of organic molecules and bacteriostatic effects.

Results and Discussion

Synthesis

Obtaining branched microstructures with a high surface-to-volume ratio is a challenge and here we achieved it by tuning crystal growth kinetic factors with the concentration of Cl^- ions in solution (see details in Supporting Information). Using a simple approach to control the release of Cl^- ions in solution we engineer the formation of hierarchically branched superstructures. The silver chloride precipitates as by-product in a reaction to produce supermolecular structures (as can be seen Scheme 1).

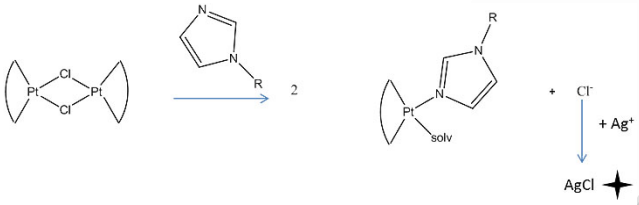

Scheme 1. Schematic representation of the synthetic strategy followed to obtain microstar-shaped AgCl particles.

In a typical experiment, $AgPF_6$ is added to a solution of the platinum complex [Pt $(\mu\text{-Cl})_2(\text{dmba})_2$] (dmba = (*N*,*N*′-dimethylbenzylamine) ■■ok?■■ in DMSO in which no precipitate is observed (structure shown in Supporting Information). Upon addition of a heterocyclic compound, delayed precipitation of AgCl occurred from co-formation and dissolution. We added the given ligand in order to shift the equilibrium towards that of the desired AgCl structures. ■■previous two sentences ok?■■ Upon reaction with compound **2** (see Scheme 1), the controlled release of the Cl^- ions and the subsequent precipitation with Ag^+ present in solution was induced. The supermolecular structures remain in solution, and AgCl precipitates were isolated by centrifugation.

The chemical composition of the precipitate was confirmed by EDX analysis, as shown in Figure 1 a. The shape is tuneable by adjusting the amount of free Cl^- ions by the addition of a heterocyclic compound, resulting in cube-like structures or overgrown octapod-shaped microstar structures (μS) Figure 1 (b–e). At low Cl^- concentrations, the cubic seeds precipitate showing already an incipient preferential growth through the cube edges (image not shown). As the ratio is increased, the concave cubes grow larger along the directions of corners up to the formation of microstars (μS). These results are associated with the two different stages involved in crystallization: nucleation and growth. The preferential overgrowth required to obtain μS is due to different energy content of atoms at corners and edges.[11] An increase above 1.0 equivalents results

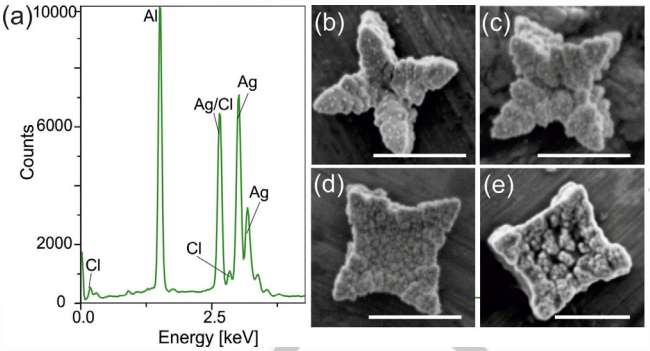

Figure 1. Synthesis of AgCl microstars. a) EDX analysis of the precipitate. All signals can be associated either to silver or to chloride, only the obtained Al-signal is due to the aluminum sample holder. b–e) The morphology of the AgCl precipitate strongly depends on the stoichiometry of heterocycles added (while keeping constant the 1:1 Ag/Cl ratio): from μS structures to concave cubes with overgrown corners, the average end-to-end dimensions were about 2 μm. Scale bars equal 1 μm.

in the formation of cubic AgCl microstructures. This preferential growth increases upon increasing the Cl^- concentration eventually leading to the formation of the octapod structures. Finally, at higher concentrations, the availability of Cl^- is so high that less selective "docking" occurs and the energy differences between the different crystal facets lose importance. Other product/solvent combinations lead to partial precipitation, but no special shapes were observed (see Figure S1, Supporting Information).

Dynamics of motion

AgCl microstars gain motility one by one after irradiation with focused UV light from a mercury arc lamp at maximum intensity (120 W, DAPI excitation 340–380 nm) (see Figure S3, Supporting Information). This can be explained by the gradient build up after the onset of light, triggering the particle motility. Those active particles undergo changes on their surface, discharging chloride ions and creating the chemical gradient to propel the particle motion. Gradient-driven motion has been discussed for motile particles mostly in the context of oxygen gradients that lead to propulsion, but other forms, such as ion gradients, have also been proposed.[10,12] Here, the gradient is caused by the released chloride ions upon irradiation of AgCl structures with UV light from a mercury arc lamp at maximum intensity. The hypothesis that a chloride ion gradient is responsible for the motion is underpinned by the observation that in high concentrations of chloride ions (such as 0.1 M KCl) UV light caused no motion.

Comparing both shapes we observed that smaller cubes rotate much faster, which is counterintuitive at first because the reaction of AgCl with light is a surface reaction; therefore, an increase in surface area should lead to an absolute increase of created product. Assuming a constant volume for both cubes and μSs, we calculated the volume/surface ratio and found, that the μS has a 1.7 times larger surface area (see Table 1). Even though the amount of product created by a larger surface may be increased, the distribution of the prod-

Table 1. Geometric properties of an exemplary cube vs. microstar (μS) of 1 μm³ volume.

	Cube	μS
Volume (*V*)	1 μm³	1 μm³
Side length (*a*)	1 μm	1.26 μm
Surface (*A*)	6 μm²	10.64 μm²
Ratio *A*/*V*	6	10.64

uct over a larger area and the changes in angular momentum cause the μSs to turn more steadily. Their different angular momentums are associated with the quadratic dependence of the distance between extremes from the central axis, and secondly, a larger surface also means a larger interaction interface with the surroundings. From now on further studies to gain more insight on the dynamics of AgCl were exclusively concentrated on μSs. This is due to their larger structure and therefore easier detection and tracking. Ballistic motion in one constant direction is rarely observed: most of the time diffusive (Figure 2a) and rotational (Figure 2b) motions were observed simultaneously.

The path of an individual particle is also highly dependent on other external influences such overlapping gradients due to the presence of adjacent particles. This confirms earlier findings of Sen's group where isolated particles showed behavior similar to Brownian motion while coupled particles exhibited significantly higher diffusion constants.[13] The translational component is characterized by plotting the different mean square displacements (MSD, for details on the formula see the Experimental Section) averaged for three different μS samples.

The results are shown in Figure 2. As can be seen there, μS exhibit a relatively straight directed motion (III) with a curved MSD over 10 s, while the other more randomly moving stars (I&II) show a much less curved MSD behavior. Similar observations can be made for the rotational component. The analysis of two differently rotating stars is presented in Figure 2b. The upper star is rotating back and forth, resulting in a non-constant "continuous angle change" ($\Delta\theta$, green curve) that reflects the increasing and diminishing of the angle respective to an initial position. A different way to characterize this motion is the "mean square angular displacement" (MSAD, equivalent to MSD for angular changes, formula in Supporting Information) which is found to be an almost straight line. On the contrary, a star performing constant rotation over a prolonged time frame is shown in red (Figure 2b).■■ok?■■ This type of rotation is characterized by a constantly increasing $\Delta\theta$ because the star is never turning backwards, which translates into a parabolic MSAD. Depending on the inherent properties of each star and its surroundings, we find different modes of motion.

Durability of motion

Considering that the mechanism powering the motion involves the slow transformation of the particle itself, additional experiments were done to determine the duration. To do so, an aqueous colloidal dispersion of the μS was placed in an inverted microscope under UV-light illumination within a flat petri dish covered to inhibit solvent evaporation and the movement was followed over time. Every 60 minutes (up to three hours), videos of particle movement were taken and evaluated. With progressing time the catalytic surface reaction modifies the

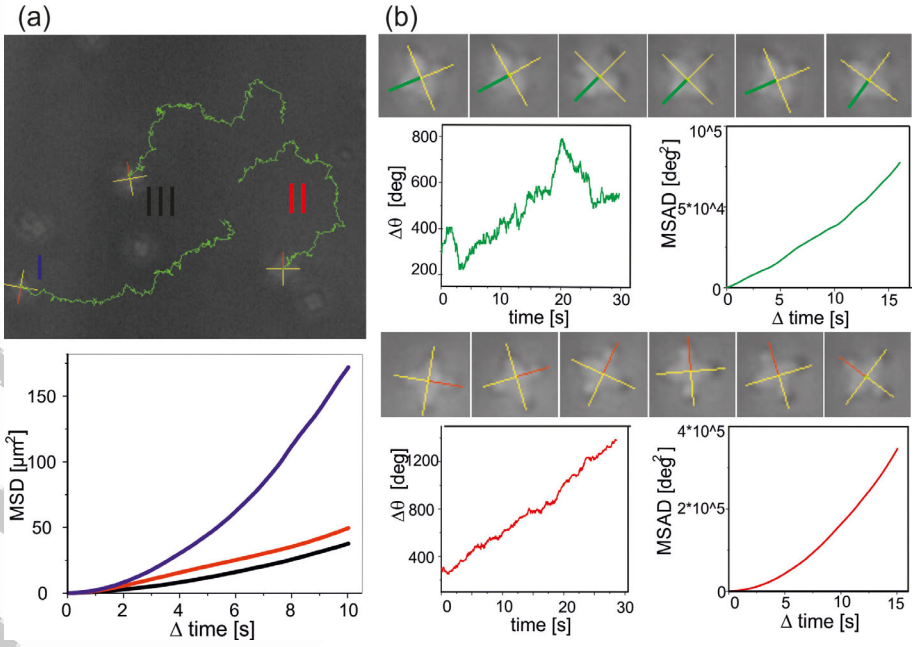

Figure 2. a) Translational component of motion—tracked enhanced Brownian diffusion of three motile AgCl μSs and the respective MSDs (blue line star I, red line star II, black line star III). b) Within the movement of a single microstar, the rotational parts were tracked and analyzed, two different kinds of rotation are displayed: the green back and forth rotating star results in a much less curved, almost straight MSAD while the red star constantly rotating in one direction results in a more curved MSAD.

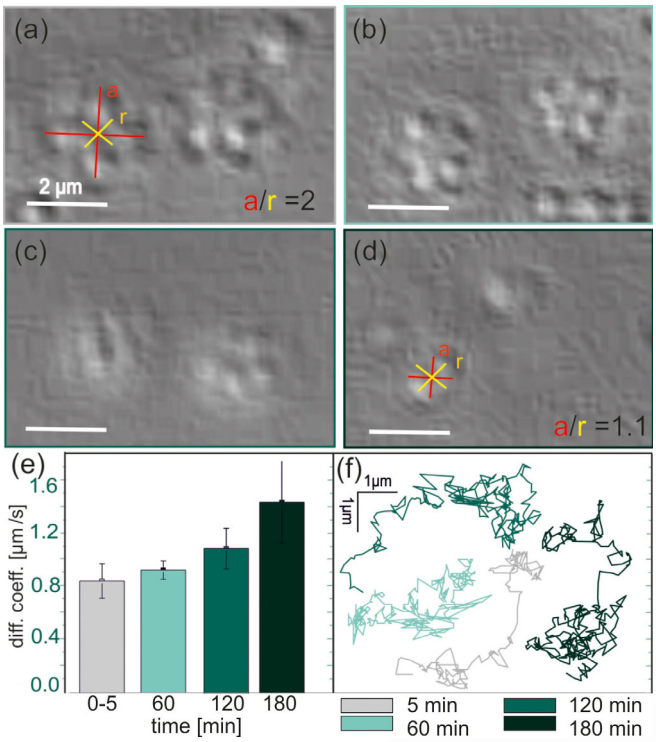

Figure 3. Lifetime and motion of light-activated µS. a–d) shape of the µS at different times: a) 5, b) 60, c) 120, d) 180 min. The images show the subsequent degradation of the µS structures due to surface modification. Ratio of arm length versus radius indicates the degradation of the µS with time. e) Speeds obtained from the MSD of minimum 3 µS at different times. f) Trajectories of exemplary µS, each track corresponds to 10 s of µS motion.

particle shape, from µS (see inset *a*/*r* in Figure 3a ■■please define variables■■) to roundish body particles resulting in the observation of mainly stubs after long periods of time (see Figure 3d).

Nevertheless, the formation of stubs after exposition for 3 h does not disrupt motion, as can be seen in the exemplary motion of the different stages shown in Figure 3e–f. The trajectories of the corresponding particles after 5, 60, 120 and 180 min are displayed in Figure 3f). The bars in Figure 3e show the different translational components of the motion. Their MSD evaluation resulted in effective diffusion coefficients, where a higher value correlates to a higher velocity. In the absence of light, particles can be stored in water for a several days without any significant morphology modification; after drying, storage was possible over month without losing shape. In dry state the only observed change was nanograin formation on the surface.

Potential environmental applications

Catalytic micromotors can be exceptional devices for environmental applications[14] by taking advantage of the spontaneous movement. In the present work, two environmental applications inherently related to the properties of AgCl were explored: I) degrading organic material[15] such as certain pollutants[16] through photocatalytic properties and II) antibacterial treatment with silver, which is widely known for its antibacterial properties, as recently demonstrated by Pané's group with silver-coated helical nanomachines.[17] ■■ok?■■ The photocatalytic activity of AgCl µS was evaluated with an aqueous so-

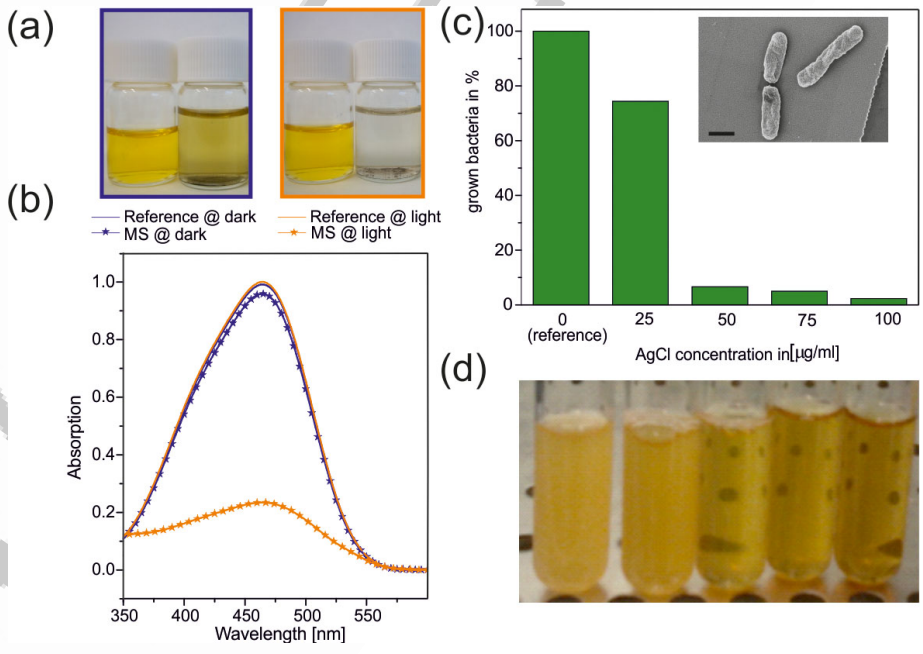

Figure 4. Environmental applications of µS: a–b) The photocatalytic activity of AgCl µS was evaluated by testing the photocatalytic degradation of methyl orange (MO) aqueous solution. a) Optical image after 3 h of irradiation; the solutions exposed to sun were almost completely colorless. The reference samples help evaluating the stability of the molecules exposed after light exposure but in absence of AgCl; it can be clearly seen that only in presence of both AgCl and light can the decomposition of the dye take place. b) Absorption spectrum of the MO samples and blank solutions. c) Inhibition of bacterial growth tested on *E. coli*, values measured by densitometry. Inset: SEM image of *E. coli* bacteria, scale bar corresponds to 1 µm. d) Optical evaluation of bacterial growth in solution. At about 50 µg mL^{-1} a threshold concentration is reached that inhibits bacterial growth.

lution of methyl orange (see Figure 4a–b). Specifically, two different solutions with identical concentrations of dyes were prepared, with and without μSs, and were exposed to sunlight irradiation while the evolution of the organic dye was followed by UV/Vis absorption spectroscopy. Two additional solutions were also prepared and kept in the absence of any light source for comparison purposes. After 3 h stored in darkness none of the two controls showed any significant change (blue framed image in Figure 4a and blue curves in b). Similar results were obtained for the sample exposed to light but in the absence of μSs. Finally, the solution containing the μSs and exposed to sunlight was found to be almost completely colorless (right sample, orange framed image Figure 4a, orange line with star symbols in b). To prove the versatility of the catalytic decomposition on different chemical structures this study was extended to methyl blue and rhodamine 6G with similar excellent results (for more details see Figure S5 in the Supporting Information).

A second set of experiments was designed and performed to demonstrate the antibacterial properties of AgCl μS. As can be seen in Figure 4, after addition of 25 $\mu g\,mL^{-1}$ μS the bacteria growth dropped by approximately 25% (confirmed by densitometry and colony counting, for details see Experimental Section). Further increase of the μS concentration to 50 $\mu g\,mL^{-1}$ inhibited the growth of *E. coli* drastically: only 6.6% of the growth was found compared to the reference sample. Further increase of the AgCl concentration hardly lowered the growth rate any further (values obtained by densitometry and colony counting confirmed those results, further details in the Supporting Information). To elucidate the mechanism of these antibacterial properties the influence of the state of the μSs (fresh or aged, and presence or absence of light) was tested, but caused almost no variation in the results. This observation leads to the conclusion that the photocatalytic processes play only a minor role for the bacteriostatic effect and the main factor seems to be the concentration of silver ions.

These observations led to the hypothesis that there is a maximum amount of soluble ion concentration in the Todd Hewitt broth (THB) medium, which is reached around 50 $\mu g\,mL^{-1}$. To verify this hypothesis the concentration of Ag^+ ions in THB was measured by ICP-MS and compared to a corresponding inorganic buffer (see Supporting Information, Figure S6). The solubility of AgCl in salt solution and THB differs strongly, probably due interactions with the organic components of THB such as complexation phenomena.

Conclusions

We have demonstrated a novel synthesis route for uniquely shaped AgCl particles and their ability to be used as light-driven micromotors. The manufacturing is based on delayed a precipitation that allows the control of precipitation dynamics and therefore offers a possibility to obtain a range of shapes from cubes and to octapod-shaped microstars. Those microstars enable us to observe the motion in pure water after UV irradiation and characterize three different modes: translation, rotation and rocking. To reach one step further we showed as a proof of concept that the AgCl microstars have potential to be applied in waste water treatment due to their versatile photocatalytic activity enabling them to degrade organic molecules. Another promising feature for waste water treatment is their bacteriostatic properties, which lead to an inhibition of bacterial growth. In conclusion, we consider that these findings broaden our knowledge of UV-driven micromotors and the novel shapes open possibilities to study shape-dependent collective behavior. However, further efforts are needed to bring this new kind of motors to the level of control that can be reached currently with other types of micromotors, such as directionality and speed control.

Experimental Section

Experimental Details

Synthesis of AgCl particles

In a typical synthesis [Pt $(\mu\text{-Cl})_2(\text{dmba})_2$] (10 mg, 0.0133 mmol) was dissolved in 4 mL DMSO. A solution of 1 equiv of an inorganic silver salt ($AgPF_6$) in 1 mL DMSO was added dropwise and stirred for 1 h protected from light. Initially no precipitation of AgCl was observed. In order to shift the equilibrium towards the products 1 equiv of bis(imidazol-l-ylmethyl)benzene or 2 equiv of imidazole were added and enhanced precipitation of AgCl was observed. The precipitate was filtered and washed with EtOH.

1,4-Bis(imidazol-l-ylmethyl)benzene (bix) was synthesized following a method published by P.K. Dhal et al.■■Please provide reference■■: 1.9 g (48 mmol) of a sodium hydride suspension in mineral oil (60%) were washed with 10 mL of dry THF under nitrogen and subsequently dissolved in 30 mL dry THF. Under a nitrogen atmosphere, imidazole (2.85 g, 44 mmol) dissolved in 15 mL of dry THF was added slowly and the mixture was allowed to stir for 30 min. a,a′-Dibromo-*p*-xylene (5.3 g, 20 mmol) in 20 mL of THF was added to the resulting suspension, which was then heated to 50 °C for minimum of 4 h. The reaction mixture was cooled with approximately 25 mL of ice water and stirred for 20 min. Then the product was extracted with chloroform (3×50 mL), and the combined organic phases were dried over anhydrous sodium sulfate. After filtration, the solvent was removed under reduced pressure and the obtained product was found to be pure in NMR analysis and used without further purification.

UV driven micromotors

Experiments were performed in a Zeiss Axiovert microscope coupled to an EXFO lamp (X-Cite) and either an AxioCam MRm or a Thorlab USB 2.0 camera. A sample holder bearing a freshly cleaned glass slide was covered by 100 μL Milli-Q water and 2 μL μS in water were added. When irradiated with white light generally no movement was observed, only after turning on the UV lamp (with DAPI filter) did the particles start to move. The particles continued their movement even after turning of the UV light for some time, indicating that the created gradient does not disappear by turning off the light.

Degradation of organic molecules

Microstars were precipitated as described previously, washed in ethanol and water and redispersed in DI water in a concentration of 0.01 $mg\,\mu L^{-1}$. Solutions of methyl orange, methyl blue and rhod-

amine 6G were prepared in a concentration of 10 mg L^{-1}. Finally to 5 mL colorant solution 30 µL of µS suspension were added, or, for blank experiments, 30 µL of pure water. A blank solution and a µS-containing solution of each colorant were kept in the dark; equally, a blank solution and a µS-containing solution without colorant ■■ok?■■ were placed under a UV lamp and another batch of blank and test solutions were placed in the sun. The degradation was found to be incomplete after 30 min, therefore the duration of the experiment was extended to 3 h when the solutions were either colorless or strongly decolorized. After that time, UV absorption was measured in the wavelength range corresponding to the colorant. Concentrations: catalyst concentration: 0.01 mg μL^{-1}; solution of organic compounds: 10 mg L^{-1}; 30 µL of catalyst concentration was added to each sample. Absorptions were measured in the ranges (depending on the colorant) shown in Table 2.

Table 2. Absorption measurements. ■■title ok?■■

Organic colorant	Initial wavelength [nm]	Final wavelength [nm]
Methyl orange	250	600
Methyl blue	250	400
Rhodamine 6G	400	600

Bactericidal effect

Several concentrations of silver nanoparticles (0, 25, 50, 75 and 100 µg mL^{-1}) were tested against *E. coli*. Therefore *E. coli* cells should always be done on freshly unfrozen cultures. ■■Please clarify. Grown from?■■ An agar plate was inoculated with 20 µL of unfrozen glycerol stock and grown overnight. A single colony was used to inoculate 100 mL of THB (containing salts, dehydrated heart infusion, yeast enriched peptone and dextrose) solution and incubated at 37 °C overnight. Density measurement gave 1.497 after 16 h. A dilution 1:10 was found to have suitable density for exponential growth (0.322) and used for further experiments. Dilutions of the same solution (10^{-1} to 10^{-6}) were inoculated on agar plates to count CFU, which resulted in 9.05×10^7 CFU mL^{-1}.■■superscript added ok here and below?■■

The interaction with silver nanoparticles was analyzed by adding silver nanoparticles to the *E. coli* solution of 9×10^7 CFU mL^{-1}.■■ The homogeneous suspensions of 0–100 µg mL^{-1} were allowed to grow overnight under agitation in an orbital shaker to avoid particle sedimentation. Optical density was measured and CFUs were counted in dilutions of 10^{-2} and 10^{-4}. To determine the light sensitivity the same protocol was followed, with the only difference that the growth occurred partially in darkness and partially under irradiation with a USB-LED lamp. To evaluate the amount of AgCl dissolved into solution, the concentration of Ag^+ ions in THB and pure inorganic buffer solution was measured. Therefore the synthesized AgCl µS were added to 5 mL solution (THB or buffer, respectively) and shaken for 8 h before centrifugation to remove all not dissolved particles. Then samples were sent to ICP-MS analysis for Ag^+ ions.

Tracking

Following reference [18], accurate tracking of the nanoparticles was performed on the recorded videos to compute the mean square displacement (MSD) and mean square angular displacements (MSAD). To achieve statistical data tracking was done automatically employing an especially developed script in Python 2.7 using the OpenCV library. First the image frame is cleaned of noise by using different types of blurring (median, Gaussian and bilateral filtering, depending on the quality of the recording), and then a gradient is applied by convoluting with the appropriate sobel kernel, which approximates the first derivative at every pixel, using a finite differences method plus Gaussian smoothing. By thresholding the absolute of this gradient the contours of the µS can be obtained and the centers are then easily calculated. Bayesian decision-making (the closest shape to a previous position is always assumed to be the correct one) enables us to accurately follow the trajectory of the detected µS. Then the MSD was approximated from the data points using Equation (2):

$$\mathrm{MSD}\ [\Delta t] = \sum_{i=0}^{N-\Delta t} \frac{r\,[i+\overrightarrow{\Delta t}-\vec{r}[i]^2}{N-\Delta t} \qquad (2)$$

where Δt is the time displacement, N is the total number of data points, and $r[i]$ is the position at time i. The effective diffusion coefficient is obtained by fitting the data to Equation (3):

$$\mathrm{MSD}\ [\tau] = 4D\tau \qquad (3)$$

which holds in this case because the movement is mainly enhanced Brownian motion. For the angle tracking a similar process is used: gradient analysis of the frames is also applied but with slightly different parameters, so that the arms of the stars are more clearly defined. By computing the four directions in which the contour is, on average, further away from the center, the four arms of every star can be distinguished at each frame, and the rotational movement tracked over time. The basic theory that describes the MSD in different types of translational motion can also be used to characterize rotational motion. A randomized spinning due to Brownian motion results in a linear mean square angular displacement, and a constantly changing angle trivially gives a parabolic shape. Using this magnitude makes it possible to easily characterize the different types of rotation. The equation is the same as for the MSD, but substituting position by angle.

Acknowledgements

All authors thank Jose Ruiz and Venancio Rodrıguez for providing the Pt-dimer and Lluis Soler for the help installing the camera. This project has been financially supported by the European Research Council (ERC) for Starting Grant 'Lab-in-a-tube and Nanorobotics biosensors; LT-NRBS' (no. 311529), the German Research Foundation (DFG, SA 2525/1-1). J.S. acknowledges the Jae-Pre fellowship from CSIC.

Keywords: antibacterial · environmental applications · photoactive colloids · self-propellers · silver chloride

[1] a) W. F. Paxton, P. T. Baker, T. R. Kline, Y. Wang, T. E. Mallouk, A. Sen, *J. Am. Chem. Soc.* **2006**, *128*, 14881 – 14888; b) D. Kagan, P. Calvo-Marzal, S. Balasubramanian, S. Sattayasamitsathit, K. M. Manesh, G.-U. Flechsig, J. Wang, *J. Am. Chem. Soc.* **2009**, *131*, 12082 – 12083; c) P. Calvo-Marzal, K. M. Manesh, D. Kagan, S. Balasubramanian, M. Cardona, G.-U. Flechsig, J. Posner, J. Wang, *Chem. Commun.* **2009**, 4509 – 4511; d) A. A. Solovev, S. Sanchez, M. Pumera, Y. F. Mei, O. G. Schmidt, *Adv. Funct. Mater.* **2010**, *20*, 2430 – 2435; e) L. Baraban, M. Tasinkevych, M. N. Popescu, S. Sanchez, S. Dietrich, O. G. Schmidt, *Soft Matter* **2012**, *8*, 48 – 52.

[2] a) R. Laocharoensuk, J. Burdick, J. Wang, *ACS Nano* **2008**, *2*, 1069 – 1075; b) W. Gao, A. Pei, R. Dong, J. Wang, *J. Am. Chem. Soc.* **2014**, *136*, 2276 – 2279; c) M. E. Ibele, Y. Wang, T. R. Kline, T. E. Mallouk, A. Sen, *J. Am. Chem. Soc.* **2007**, *129*, 7762 – 7763.
[3] S. Tottori, L. Zhang, F. Qiu, K. K. Krawczyk, A. Franco-Obregón, B. J. Nelson, *Adv. Mater.* **2012**, *24*, 811 – 816.
[4] a) X. Ma, A. Jannasch, U.-R. Albrecht, K. Hahn, A. Miguel-López, E. Schäffer, S. Sánchez, *Nano Lett.* **2015**, *15*, 7043 – 7050; b) X. Ma, X. Wang, K. Hahn, S. Sánchez, *ACS Nano* **2016**, *10*, 3597 – 3605; c) L. K. E. A. Abdelmohsen, M. Nijemeisland, G. M. Pawar, G.-J. A. Janssen, R. J. M. Nolte, J. C. M. van Hest, D. A. Wilson, *ACS Nano* **2016**, *10*, 2652 – 2660; d) D. Walker, B. T. Käsdorf, H.-H. Jeong, O. Lieleg, P. Fischer, *Sci. Adv.* **2015**, *1*, e1500501.
[5] a) T. D. Frank, *Condens. Matter Phys.* **2014**, *17*, 43002; b) G. Zhao, M. Pumera, *J. Phys. Chem. B* **2012**, *116*, 10960 – 10963.
[6] M. Guix, C. C. Mayorga-Martinez, A. Merkoçi, *Chem. Rev.* **2014**, *114*, 6285 – 6322.
[7] J. Palacci, S. Sacanna, A. P. Steinberg, D. J. Pine, P. M. Chaikin, *Science* **2013**, *339*, 936 – 940.
[8] a) Y. Hong, M. Diaz, U. M. Córdova-Figueroa, A. Sen, *Adv. Funct. Mater.* **2010**, *20*, 1568 – 1576; b) S. Giudicatti, S. M. Marz, L. Soler, A. Madani, M. R. Jorgensen, S. Sanchez, O. G. Schmidt, *J. Mater. Chem. C* **2014**, *2*, 5892 – 5901; c) M. Enachi, M. Guix, V. Postolache, V. Ciobanu, V. M. Fomin, O. G. Schmidt, I. Tiginyanu, *Small* **2016**, *12*, 5497 – 5505.
[9] a) W. Duan, M. Ibele, R. Liu, A. Sen, *Eur. Phys. J. E* **2012**, *35*, 77; b) M. E. Ibele, P. E. Lammert, V. H. Crespi, A. Sen, *ACS Nano* **2010**, *4*, 4845 – 4851; c) M. Ibele, T. E. Mallouk, A. Sen, *Angew. Chem. Int. Ed.* **2009**, *48*, 3308 – 3312; *Angew. Chem.* **2009**, *121*, 3358 – 3362.
[10] J. L. Anderson, *Annu. Rev. Fluid Mech.* **1989**, *21*, 61 – 99.
[11] H. Gatemala, C. Thammacharoen, S. Ekgasit, *CrystEngComm* **2014**, *16*, 6688 – 6696.
[12] A. Brown, W. Poon, *Soft Matter* **2014**, *10*, 4016 – 4027.
[13] H. Wang, G. Zhao, M. Pumera, *J. Am. Chem. Soc.* **2014**, *136*, 2719 – 2722.
[14] a) L. Soler, S. Sanchez, *Nanoscale* **2014**, *6*, 7175 – 7182; b) M. Guix, J. Orozco, M. García, W. Gao, S. Sattayasamitsathit, A. Merkoçi, A. Escarpa, J. Wang, *ACS Nano* **2012**, *6*, 4445 – 4451; c) W. Gao, A. Pei, J. Wang, *ACS Nano* **2012**, *6*, 8432 – 8438.
[15] a) C. An, R. Wang, S. Wang, X. Zhang, *J. Mater. Chem.* **2011**, *21*, 11532 – 11536; b) P. Wang, B. Huang, Z. Lou, X. Zhang, X. Qin, Y. Dai, Z. Zheng, X. Wang, *Chem. Eur. J.* **2010**, *16*, 538 – 544.
[16] F. Mushtaq, A. Asani, M. Hoop, X.-Z. Chen, D. Ahmed, B. J. Nelson, S. Pané, *Adv. Funct. Mater.* **2016**, *26*, 6995 – 7002.
[17] M. Hoop, Y. Shen, X.-Z. Chen, F. Mushtaq, L. M. Iuliano, M. S. Sakar, A. Petruska, M. J. Loessner, B. J. Nelson, S. Pané, *Adv. Funct. Mater.* **2016**, *26*, 1063 – 1069.
[18] G. Dunderdale, S. Ebbens, P. Fairclough, J. Howse, *Langmuir* **2012**, *28*, 10997 – 11006.

Manuscript received: October 17, 2016
Accepted Article published: November 21, 2016
Final Article published: ■■ ■■, 0000

FULL PAPER

Micromotors

Juliane Simmchen, Alejandro Baeza, Albert Miguel-Lopez, Morgan M. Stanton, Maria Vallet-Regi, Daniel Ruiz-Molina, Samuel Sánchez*

■■ – ■■

Dynamics of Novel Photoactive AgCl Microstars and Their Environmental Applications

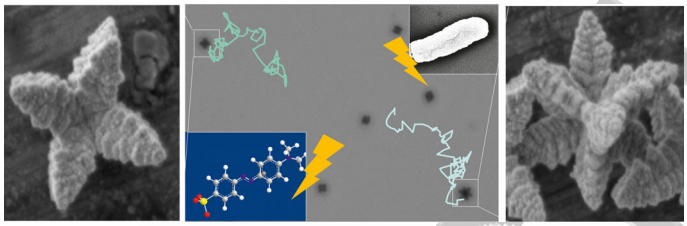

■■Please provide a short text for the table of contents■■

Self-propelling AgCl micromotors from J. Simmchen @MPI IS Tue SPACE RESERVED FOR IMAGE AND LINK

Share your work on social media! *ChemNanoMat* has added Twitter as a means to promote your article. Twitter is an online microblogging service that enables its users to send and read text-based messages of up to 140 characters, known as "tweets". Please check the pre-written tweet in the galley proofs for accuracy. Should you or your institute have a Twitter account, please let us know the appropriate username (i.e., @accountname), and we will do our best to include this information in the tweet. This tweet will be posted to the journal's Twitter account @ChemNanoMat (follow us!) upon online publication of your article, and we recommended you to repost ("retweet") it to alert other researchers about your publication.

Please check that the ORCID identifiers listed below are correct. We encourage all authors to provide an ORCID identifier for each coauthor. ORCID is a registry that provides researchers with a unique digital identifier. Some funding agencies recommend or even require the inclusion of ORCID IDs in all published articles, and authors should consult their funding agency guidelines for details. Registration is easy and free; for further information, see http://orcid.org/.

Dr. Juliane Simmchen
Dr. Alejandro Baeza
Albert Miguel-Lopez
Dr. Morgan M. Stanton
Prof. Dr. Maria Vallet-Regi
Dr. Daniel Ruiz-Molina
Dr. Samuel Sánchez